Early Solar System hydrothermal activity in chondritic asteroids on 1–10-year timescales

Kathryn A. Dyl[a,b,1], Addi Bischoff[c], Karen Ziegler[a,d], Edward D. Young[a,e], Karl Wimmer[f], and Phil A. Bland[b]

[a]Department of Earth and Space Sciences and [e]Institute of Geophysics and Planetary Physics, University of California, Los Angeles, CA 90095; [b]Department of Applied Geology, Curtin University of Technology, Perth, WA, 6845 Australia; [c]Institut für Planetologie, 48149 Münster, Germany; [d]Institute of Meteoritics, University of New Mexico, Albuquerque, NM 87131; and [f]86720 Noerdlingen, Germany

Edited by Ikuo Kushiro, University of Tokyo, Tsukuba, Japan, and approved September 25, 2012 (received for review May 9, 2012)

Chondritic meteorites are considered the most primitive remnants of planetesimals from the early Solar System. As undifferentiated objects, they also display widespread evidence of water–rock interaction on the parent body. Understanding this history has implications for the formation of planetary bodies, the delivery of water to the inner Solar System, and the formation of prebiotic molecules. The timescales of water–rock reactions in these early objects, however, are largely unknown. Here, we report evidence for short-lived water–rock reactions in the highly metamorphosed ordinary chondrite breccia Villalbeto de la Peña (L6). An exotic clast (d = 2cm) has coexisting variations in feldspar composition and oxygen isotope ratios that can only result from hydrothermal conditions. The profiles were modeled at T = 800 °C and $P(H_2O)$ = 1 bar using modified grain-boundary diffusion parameters for oxygen self-diffusion and reaction rates of $NaSiCa_{-1}Al_{-1}$ exchange in a fumarole. The geochemical data are consistent with hydrothermal activity on the parent body lasting only 1–10 y. This result has wide-ranging implications for the geological history of chondritic asteroids.

aqueous alteration | metamorphism | albitization | L-chondrites | inclusions

Chondritic meteorites, undifferentiated samples from early Solar System planetesimals, display widespread evidence of aqueous alteration and water–rock interaction on their precursor planetesimals (1, 2). Elucidating the detail of water–rock interaction is essential to an understanding of Solar System formation. Isotope-specific photodissociation of CO by UV light appears to explain the oxygen isotope ratios of the Sun, meteorites, and planets by reactions between ^{16}O-rich solids and ^{17,18}O-rich water (3). Reactions between rock and water also produced prebiotic molecules, such as amino acids and nitrogenous bases, in planetesimals (4, 5). Chondrites provide the opportunity to identify and constrain these fundamental processes. The key to accomplishing this is a detailed model of asteroid evolution combining geophysical and geochemical conditions. At present, this is hampered by the inability to define the timescales of aqueous alteration relevant to planetesimals.

Carbonaceous chondrites experienced extensive aqueous alteration, resulting in hydrated silicates and carbonate minerals (1). Models of asteroid hydrothermal alteration have become increasingly sophisticated (6, 7), with recent work even suggesting the formation of hydrospheres in water-rich asteroids (8). However, poorly constrained input parameters have prevented a consensus on even the most fundamental of processes. This has also meant that we are unable to easily apply observations of fluid-assisted metamorphism in meteorites to the size scale of planetesimal parent bodies. A major step forward in this regard would be to constrain reaction timescales, but simple extrapolation from terrestrial observations is problematic; reaction rates and mechanisms of serpentinization vary by orders of magnitude in laboratory and field measurements (9). The ^{53}Mn–^{53}Cr short-lived nuclide geochronometer has been used to date the formation of secondary carbonate minerals, and with sufficient resolution, and enough ages, this would allow reaction rates to be constrained. However, ^{53}Mn–^{53}Cr ages range from before the formation of calcium–aluminum-rich inclusions (CAIs), nominally the oldest objects in the Solar System, to >8 Ma after the first solids (10, 11). If we take these ages at face value, it implies that aqueous alteration began before chondritic parent bodies had formed and persisted for timescales that violate many other constraints (e.g., plausible serpentinization reaction rates; available heat sources within chondritic parent bodies). An alternate explanation would be that there are factors that complicate the straightforward application of ^{53}Mn–^{53}Cr to dating alteration duration.

The history of water–rock interaction on ordinary chondrites (OCs) is even less clear. OCs experienced prolonged thermal metamorphism on their parent bodies, as evidenced by a broad range of textures and recrystallization fabrics (12). Type 6 chondrites, those that underwent extensive thermal metamorphism, experienced temperatures >800 °C for extended periods of time, as long as ∼60 Ma in some models (13). There is also growing evidence, however, for the role of volatiles and/or fluids in this metamorphism. Correlations in oxidation state (14), the presence of smectite in OC matrices (15), the presence of "bleached chondrules" depleted in soluble elements (16), and variations in feldspar composition (17) have all been used as evidence for aqueous alteration on the parent body. Furthermore, oxygen isotope ratios are heterogeneous at the kilometer scale in these objects, consistent with small variations in reactions between rock and a volatile phase (18). The role of water in thermal metamorphism and reaction timescales cannot be constrained quantitatively by these lines of evidence.

A unique opportunity to probe the conditions of metamorphism on OCs is afforded by an exotic plagioclase-rich clast in the Villalbeto de la Peña (VP) meteorite (L6). The object, shown in Fig. 1, is composed primarily of a fine-grained feldspathic matrix. Micron-sized Cr-rich spinel, kamacite, taenite, and troilite are interspersed throughout. A coarse-grained rim (grain size ∼50 μm, average width ∼100 μm) is observed at the host–clast interface. The composition varies between the host (∼An_{10}) and clast (∼An_{55}), with a diffusion profile extending ∼500 μm into the inclusion. This is also accompanied by increased maskelynization of the feldspar clast, which is a compositionally controlled process resulting from shock event(s) postdating metamorphism (19). Feldspar in the coarse-grained rim is Na-rich (∼An_{12}), indistinguishable from plagioclase grains in the host meteorite. The sharp boundary between the two lithologies, intersecting shock veins through the object, and the presence of a recrystallized rim suggest that the object was incorporated into the ordinary chondrite parent body before metamorphism.

Author contributions: K.A.D. and E.D.Y. designed research; K.A.D., A.B., K.Z., and E.D.Y. performed research; K.W. contributed new reagents/analytic tools; K.A.D., A.B., K.Z., and E.D.Y. analyzed data; and K.A.D. and P.A.B. wrote the paper.

The authors declare no conflict of interest.

This article is a PNAS Direct Submission.

[1]To whom correspondence should be addressed. E-mail: katie.dyl@gmail.com.

 www.pnas.org/cgi/doi/10.1073/pnas.1207475109

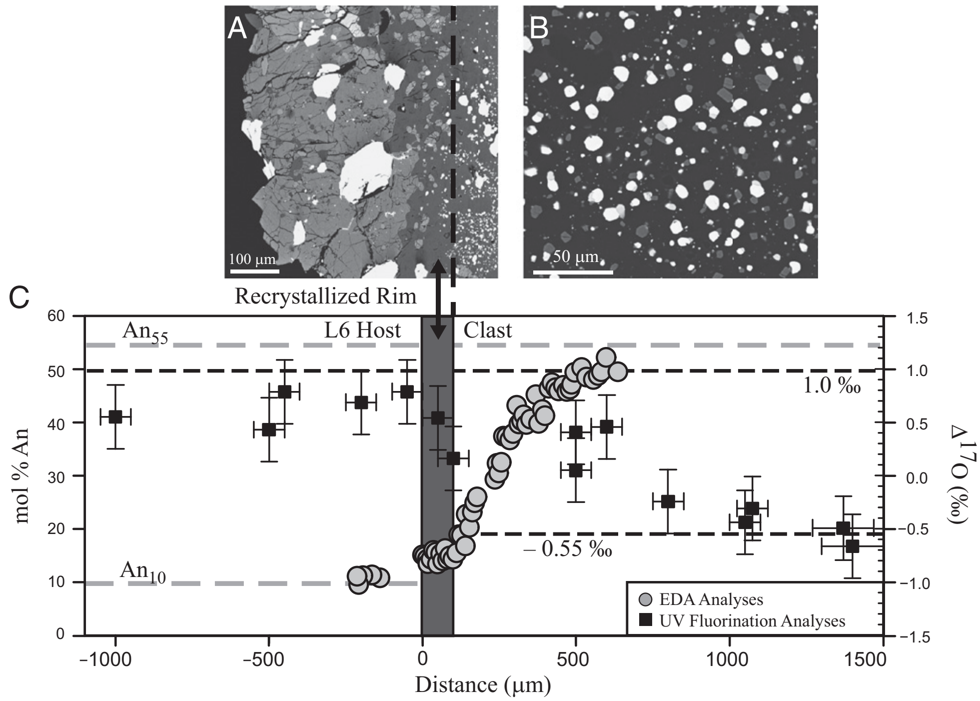

Fig. 1. Exotic inclusion in VP meteorite displaying coexisting variations in feldspar composition and oxygen isotope ratio. (*A*) Backscatter electron image (BSE) of the host–fragment interface, characterized by a recrystallized rim of feldspar (dark gray) and olivine (light gray). White inclusions are metal. The olivine is compositionally identical to that of the OC host. (*B*) BSE image of the VP clast interior. It is characterized by a fine-grained feldspathic groundmass. μm-scale inclusions of kamacite and taenite (white), chromite and Fe-sulfides (gray) are observed. (*C*) $\Delta^{17}O$ (black squares) and composition (mol % An, gray circles) as a function of distance across the host–clast interface. The values for the host meteorite and clast interior are indicated with dashed lines. Errors for feldspar analyses are within the symbols. UV laser ablation–fluorination analyses have an estimated error of ±0.3% in $\Delta^{17}O$.

Results

Measurements of the clast and host using IR CO_2 laser-assisted fluorination verify a 1.8% difference in $\Delta^{17}O$ between the L-chondrite host ($\Delta^{17}O$ ~1%) and clast ($\Delta^{17}O$ ~–0.55%) (Table 1) (20). In addition, a fragment containing both host and clast material from VP was measured in situ via UV laser ablation–fluorination (*Methods*) to determine if oxygen isotope ratios varied across the object. This technique is the only one available that can make such measurements to high precision. The varying composition of feldspar, micrometer-scale inclusions, and small variance in $\Delta^{17}O$ preclude the use of other in situ mass spectrometry techniques (e.g., secondary ion mass spectrometry, SIMS). The laser ablation–fluorination data reveal a clear isotopic gradient, indicating that exchange occurred (Table 1; Figs. 1 and 2). Analyses of the interior clast agree with the CO_2 laser-assisted fluorination data. We find that the recrystallized rim is indistinguishable from the host meteorite in oxygen isotopic ratio and observe no $\Delta^{17}O$ variation in the host meteorite within given errors. In the clast, however, there is a clear decrease in $\Delta^{17}O$ as a function of distance from the host (Fig. 1). The gradient in $\Delta^{17}O$ extends 1,000–1,500 μm into the inclusion. This is 3× larger than the extent of compositional variation measured. As Fig. 2 illustrates, the data fall along a mixing line in 3-isotope space between the recrystallized rim/host and the clast interior.

The two exchange reaction profiles observed in Fig. 1, albite–anorthite substitution ($NaSiCa_{-1}Al_{-1}$) and oxygen self-diffusion ($^{18}O^{16}O_{-1}$) and ($^{17}O^{16}O_{-1}$), were modeled to characterize and quantify the duration of metamorphism this clast must have experienced in its parent body. Several different scenarios have been considered using experimentally determined diffusion coefficients: "dry" versus "wet" conditions, the effects of hydrostatic pressure, and diffusion along grain boundaries (*Methods*) (21–26).

In Fig. 3 we compare the diffusion models under hydrothermal conditions with other types of metamorphism using an Arrhenius plot. High-temperature thermal metamorphism alone cannot

Table 1. Oxygen isotope results of VP host meteorite and clast

Sample	Distance (μm)	$\delta^{18}O$ (%)	$\delta^{17}O$ (%)	$\Delta^{17}O$ (%)	err ($\Delta^{17}O$) (%)
Host	−1,000	5.2	3.1	0.4	0.3
Host	−500	5.1	3.4	0.8	0.3
Host	−450	5.7	3.6	0.7	0.3
Host	−200	5.8	3.8	0.8	0.3
Host	−50	6.0	3.7	0.6	0.3
Host	**N/A**	**4.75**	**3.56**	**1.05**	**0.03**
		5.19	**3.88**	**1.14**	**0.03**
Fragment	50	6.4	3.9	0.5	0.3
Fragment	100	6.2	3.5	0.2	0.3
Fragment*	500	5.2	2.8	0.0	0.3
Fragment	500	6.3	3.7	0.4	0.3
Fragment	600	6.1	3.6	0.5	0.3
Fragment	800	6.4	3.1	−0.2	0.3
Fragment	1,075	6.4	3.0	−0.3	0.3
Fragment	1,050	6.5	2.9	−0.4	0.3
Fragment	1,370	6.5	2.9	−0.5	0.3
Fragment	1,400	6.4	2.7	−0.7	0.3
Fragment	**N/A**	**6.25**	**2.72**	**−0.58**	**0.03**
		6.63	**2.96**	**−0.54**	**0.03**

Boldface indicates IR laser–fluorination data (19); all other data were measured via UV laser ablation–fluorination. The error given for $\Delta^{17}O$ is the external precision of the technique. For UV laser ablation–fluorination analyses, error in $\delta^{18}O$ is ±0.1% and error in $\delta^{17}O$ is ±0.2%.

*Sample is light and shows evidence of mass-dependent fractionation. This has no effect on the $\Delta^{17}O$ value.

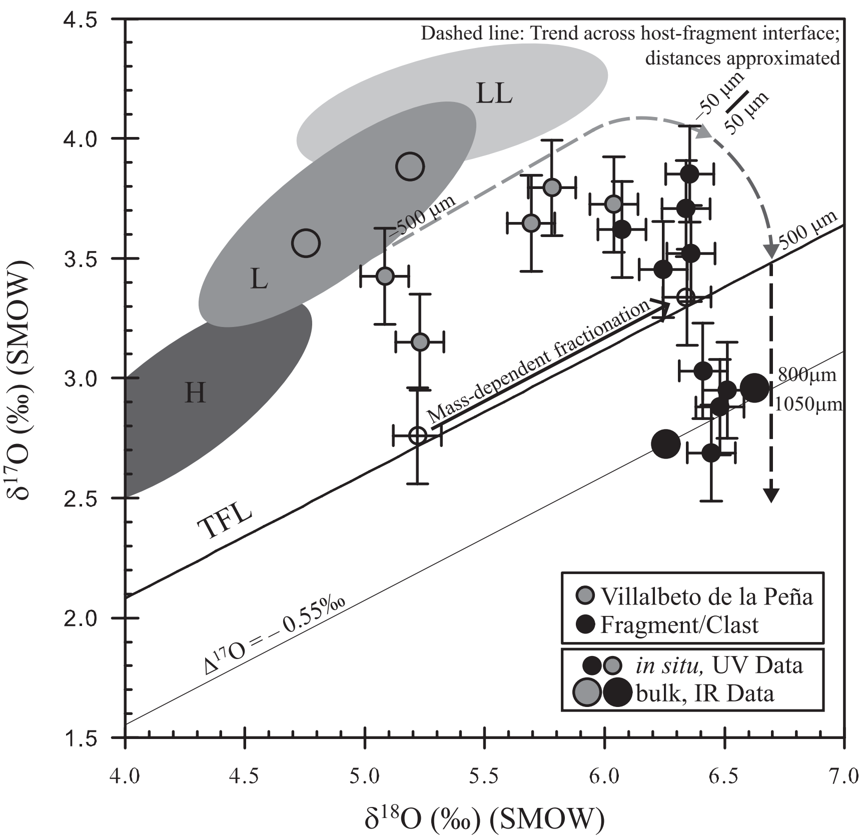

Fig. 2. Oxygen isotopic composition of VP and clast in 3-isotope space ($\delta^{17}O$ versus $\delta^{18}O$). Fluorination analyses of host material are gray circles; clast material is represented by black circles. The size indicates bulk analyses (large: CO_2 laser fluorination) or in situ analyses (small: UV laser ablation–fluorination). For one data point (open circle), mass fractionation during analysis occurred, which resulted in low $\delta^{18}O/\delta^{17}O$ values; we indicate this mass-fractionation shift and also the expected location of the data point ($\Delta^{17}O$ remains constant). Ellipses correspond to the regions where H, L, and LL ordinary chondrites plot (20). The bold line corresponds to the terrestrial mass-fractionation line. The solid below that is the mass-dependent fractionation line corresponding to $\Delta^{17}O$ = −0.55%. The dashed line illustrates the distance from the host–clast interface for the data points. The $\delta^{18}O$–$\delta^{17}O$ values also vary with distance, supporting the trend in $\Delta^{17}O$ measured by UV laser ablation–fluorination.

reproduce our coexisting geochemical trends. Even at peak temperatures (>800 °C) of ordinary chondrite metamorphism, we observe that the diffusion coefficient D required to explain the rate-limiting Si diffusion and that required for O self-diffusion differ by ~10^6 under dry conditions. Therefore, the timescale required to reproduce the compositional variation in the feldspar is three orders of magnitude greater than that required by the oxygen isotope variations. Under hydrothermal conditions, however, this is not the case. Oxygen self-diffusion and the coupled exchange reaction occur over similar timescales in the presence of water. A decrease in $P(H_2O)$ results in a decrease in the diffusivity of oxygen by 1–2 orders of magnitude (decreasing more at lower T). It is also clear from Fig. 3 that oxygen transport will be dominated by grain-boundary diffusion, not volume diffusion, in this multigrained object. The effect of $P(H_2O)$ on oxygen grain-boundary diffusion in feldspar is unknown. However, experiments using other species (K^+, Ca^{2+}) suggest that the difference between water-present and water-absent conditions is modest at best (a factor of 5 lower) (24). Therefore, the fact that we could not calibrate grain-boundary diffusion for $P(H_2O)$ should not impact our results to a significant degree.

Diffusion profiles were calculated to fit the data across a range of timescales, taking into account both the effects of grain-boundary diffusion and $P(H_2O)$ for oxygen (*Methods*). The data and model curves are presented in Fig. 4. To reproduce both the compositional variation and $\Delta^{17}O$ profile at a temperature of 800 °C and $P(H_2O)$ = 1 bar, 1–10 y are required. This temperature is consistent with several different estimates of peak temperature during metamorphism (13, 27); the absence of hydrated minerals (i.e., serpentine, mica) in VP is consistent with this choice, as is the low $P(H_2O)$ used in the calculations. Whereas a lower temperature below estimates for peak metamorphic temperatures requires longer timescales of alteration, the effect is not large. For example, at T = 700 °C the requisite diffusion time is 10–15 y. It is only below ~625 °C where timescales in excess of 100 y are required. Although no available geothermometer indicates such low peak metamorphic temperatures for type 6 OCs, the result would remain robust: Across the range of temperatures consistent with the type 6 mineralogy and petrography, fluid-assisted metamorphism was geologically instantaneous.

Discussion

The reaction textures in VP are consistent with observations of hydrothermal experiments and show that albitization is a result of coupled dissolution–reprecipitation reactions (28). The external dimensions of the crystals are preserved as the reaction front proceeds from the host–clast interface and into the object. In the VP clast, the recrystallization rim is evidence of these surface-mediated reactions. Given the textural associations, the diffusion modeling (indicating wet alteration), and the close correlation between elemental and $\Delta^{17}O$ profile model curves (both indicating the same short reaction timescale), it appears likely that VP was exposed to an H_2O vapor phase at high T (~800 °C) for a period of 1–10 y. Whereas thermal metamorphism may have persisted on longer timescales, the volatile phase can only have been present for a short period. The preservation of millimeter-scale oxygen isotope variation in feldspar at high T is also consistent with rapid water–rock reactions in the parent body (29).

These extremely short hydrothermal reaction timescales should be considered against a background of information from short-lived radioactive isotopic systems to understand the timing and mechanisms of water–rock interaction in OC parent bodies. Initial $^{129}I/^{127}I$ ratios of chondrules in the Semarkona (LL3.0) chondrite give an age range of ~10 Ma (30). The oldest ages are attributed to formation and the youngest to aqueous alteration. This has

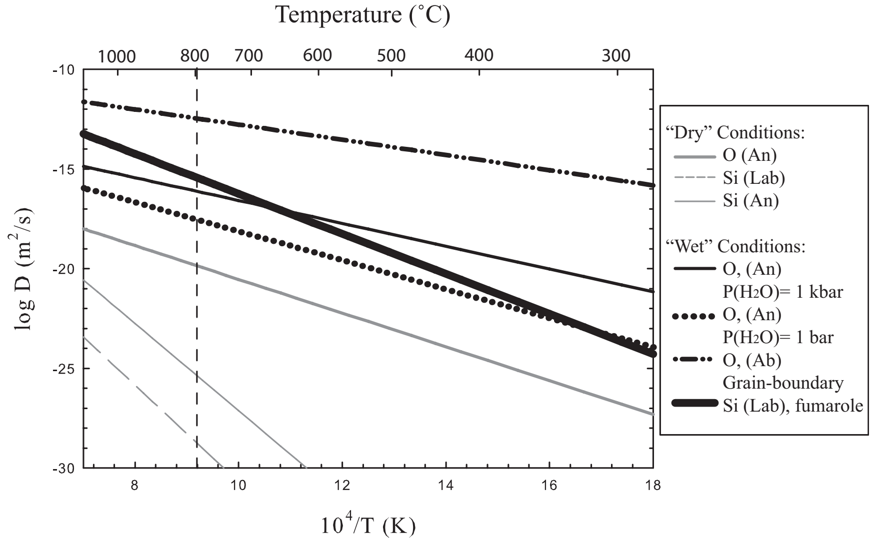

Fig. 3. Arrhenius plot of oxygen and silicon diffusion in feldspar under various metamorphic conditions. The temperature range of 300–1000 °C is consistent with the range of temperatures OCs experienced during metamorphism. The dashed vertical line at 800 °C indicates the temperature consistent with peak metamorphism in L chondrites (13, 27). Anhydrous, or dry, conditions are plotted in gray, whereas hydrothermal or wet conditions are plotted in black. The effect of $P(H_2O)$ is also considered. Grain-boundary diffusion data are only available for oxygen under hydrothermal conditions in albite. A physical grain-boundary width ϕ = 5 nm is used to plot grain-boundary diffusion of oxygen.

been interpreted as the duration of hydrothermal processes on the parent body (31).

Furthermore, halite crystals with fluid inclusions are observed in highly metamorphosed OCs (32) and have been dated using the ^{129}I–^{129}Xe chronometer. Recent work argues that these crystals are exogenous (33). However, if they are products of hydrothermal alteration, they provide constraints for comparisons to the conditions affecting the clast in this study. The initial $^{129}I/^{127}I$ in halite for Zag (H5) is close to the initial Solar System value, implying aqueous alteration within 2 Ma of CAI formation (34). Halite from Monahans (H5) has a formation age of 4,561 Ma (∼6 Ma after CAI formation). Later formation ages of ∼8 Ma after CAIs are obtained for both meteorites if an inherited $^{129}Xe^*$ component is assumed to be present (35). The retention of $^{129}Xe^*$ in halide also suggests that aqueous activity ended quickly (i.e., evaporation into space).

These million-year alteration timescales are not restricted to ordinary chondrite metamorphism. The ^{53}Mn–^{53}Cr short-lived chronometer is commonly used to date aqueous alteration in carbonaceous chondrites. Observed ranges in initial $^{53}Mn/^{55}Mn$ ratios in carbonates correspond to alteration timescales of ∼4 Ma in CM meteorite parent bodies (11) and up to ∼8 Ma in those from the Kaidun breccia (36). These ages are also thought to record the duration of aqueous alteration on planetesimals.

Given these observations, our data would suggest a cumulative record of episodic hydrothermal activity with individual pulses of hydrothermal activity lasting as briefly as a few years. These results indicate that fluid-assisted metamorphism on asteroids should not be considered as continuous, protracted events, but rather as the cumulative effects of episodic changes. Multiple episodes of heating and/or interaction with a volatile phase may be recorded in meteorites. These events were apparently ephemeral, occurring on timescales many orders of magnitude shorter than the million-year timescales implied by short-lived radioisotope chronometers. In ordinary chondrites, the various ages may represent multiple episodes of fluid–rock interaction, implying heterogeneous alteration in planetesimals. Another possibility is that the later dates record the remobilization of fluids during impact events rather than prolonged and variable hydrothermal alteration.

Reconciling short-duration hydrothermal events with the effects of internal heating by the most likely heat source in primitive planetesimals, decay of ^{26}Al ($t_{1/2} = 0.7$ Ma), requires the presence of an aqueous phase deep within a parent body (where type 6 chondrites are hypothesized to form). Such short periods of water–rock interaction could be explained via late-stage episodic release of an aqueous phase from the interior, implying that ordinary chondrites accreted wet. Alternatively, impacts with H_2O-bearing planetesimal(s) could explain short pulses of water–rock reaction. This would potentially provide both the high temperatures and transient volatile phase needed. The presence of exotic clasts also suggests metamorphism in a regolith or near-surface location, consistent with observations in other studies of OC metamorphism (27).

Methods

UV Laser Ablation–Fluorination. We obtained data for VP and the exotic clast using UV laser ablation–fluorination (37). This system offers the unique ability to obtain the oxygen isotopic gradient across the clast and the L6 OC host with both the spatial information and precision required. SIMS cannot attain the precision required to discern between the two materials. Furthermore, the fine-grained nature of the inclusion, poikilitic phases, and varying feldspar compositions cause spurious shifts in measured $^{18}O/^{16}O$ and $^{17}O/^{16}O$ due to uncontrolled matrix effects.

Two datasets were obtained over a 1–2-wk period. A 213-nm neodymium: yttrium–aluminum–garnet laser is operated at 20 W at a pulse rate of 5 Hz for 3 min. For all but one standard and sample analysis, trenches (100 μm × 600 μm) were ablated. Ablation trenches were made parallel to the host–inclusion boundary to maximize spatial resolution.

Fluorine reactant remaining is converted to $Br_{2(l)}$ in a chemical trap (KBr salt at 150 °C). Oxygen sample gas is isolated using $N_{2(l)}$ and frozen onto a Si-gel substrate. Helium carrier flow is then used to cryofocus this sample on a second Si-gel trap. A 10-m PLOT (porous layer open tubular) column (5-Å molecular sieve) at 30 °C separates contaminants (i.e., NF_3) from the sample gas, which is subsequently injected via an open split into a ThermoFinnigan 253 mass spectrometer. Oxygen reference gas is injected both before and after the sample gas to ensure accuracy.

We included a chip of San Carlos olivine standard in the sample chamber with the meteorite sample during each analytical session. Our standard analyses were relatively high in $\delta^{17,18}O$ relative to accepted values, potentially due to spontaneous low levels of reaction between reagent $F_{2(g)}$ and minor phases in the adjacent meteorite sample that are susceptible to fluorination

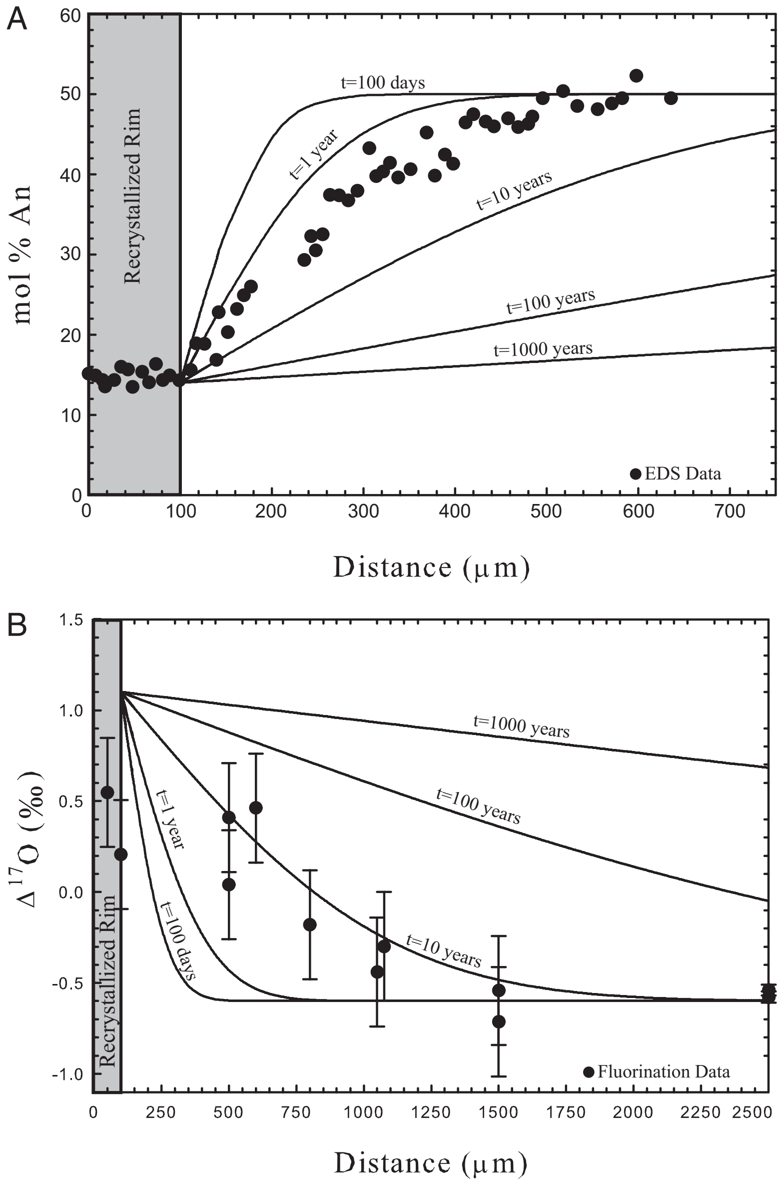

Fig. 4. Diffusion profiles fit to the compositional data (*A*) and oxygen UV laser ablation data (*B*). The coarse-grained rim is the shaded gray area. Calculations performed at T = 800 °C and $P(H_2O)$ = 1 bar. Solid lines correspond to calculations at the indicated timescales of diffusion/reaction. Results are consistent for both geochemical profiles. Timescales of 1–10 y are implied by the calculations.

in the absence of laser ablation (F_2 is known to react spontaneously with K-feldspar). We therefore normalized our results to a $\delta^{18}O$ of 5.2‰ for SC olivine. This correction was made in addition to the standard blank correction accounting for leaks to atmosphere.

Diffusion Modeling. Table 2 provides a summary of the experimentally determined pre-exponential (D_o) and activation energies (E_a) defining the temperature dependence of diffusion coefficients for oxygen and silicon in feldspar used in the calculations (21–26). For silicon under hydrothermal conditions, we used reaction rates measured from controlled experiments in a fumarole (26). To compare oxygen self-diffusion to the experimental conditions, data can be modified to model a $P(H_2O)$ = 1 bar by accommodating the linear relationship between D and $P(H_2O)$ with the following equation (25):

$$E^* = E - \alpha \times 973 \times \ln\left(\frac{f_{H_2O}(P,T)}{f_{H_2O}(1\text{kbar},T)}\right) \quad [1]$$

A hydrostatic pressure of 1 bar, as assumed here for diffusion calculations, would be found at the center of a body with radius of ~10 km. In a 100-km-sized body, this would correspond to the outermost ~10 km, consistent with asteroidal regolith (and consistent with the exotic clasts found in VP).

Diffusion profiles were calculated using the solutions for Fick's second law; the compositional profile was modeled using the reaction rate

Table 2. Experimental data used in calculations

Mineral	Species	Media	Temperature (°C)	D_o (m^2/s)	E (kJ/mol)	Refs.
Labradorite	^{30}Si	CO_2	1055–1143	5.70×10^{-6}	419	22
Labradorite	$NaSiCa_{-1}Al_{-1}$	Fumarole gas	620, 910	6.20×10^{-7}	192	27
Anorthite	^{18}O	$CO + CO_2$	1008–1295	8.40×10^{-13}	162	23
Labradorite	^{18}O	H_2O = 1 kbar	550–700	9.82×10^{-11}	130.6	24
		H_2O = 1 bar	—	9.82×10^{-11}	157.9	26
Albite: Grain boundary	^{18}O	H_2O = 1 kbar	600–800	1.10×10^{-9}	73	25

whereas oxygen self-diffusion was modeled using $P(H_2O) = 1$ bar. A temperature of 800 °C is assumed. The concentration of the species of interest (C) varies as a function of distance between the host–clast boundary (x) via the relation

$$\frac{C(x,t) - C_{clast}}{C_{host} - C_{clast}} = erfc\left(\frac{x}{2(Dt)^{1/2}}\right); \; erfc(x) = \frac{2}{\sqrt{\pi}}\int_0^x e^{-t^2}dt. \quad [2]$$

We assume a semi-infinite source and the "bulk" CO_2 laser fluorination data points as boundary conditions. Oxygen isotope diffusion was modeled using a bulk diffusivity D_{bulk}:

$$D_{bulk} = D'\varphi/a + D_{vol}(1 - \varphi/a), \quad [3]$$

where D' is the grain-boundary diffusion coefficient, D_{vol} is the volume diffusion constant, ϕ is the physical grain-boundary width (typically <5 nm), and a is the typical grain size. We have used a grain size of 1 μm, consistent with the fine-grained nature of the clast.

ACKNOWLEDGMENTS. This work was funded by NASA Cosmochemistry (E.D.Y.). K.A.D. and P.A.B. acknowledge the UK Science and Technology Research Council and the Australian Research Council Laureate Fellowship scheme for supporting part of this work.

1. Zolensky ME, McSween HY (1988) Aqueous alteration. *Meteorites and the Early Solar System*, eds Kerridge JF, Matthews MS (Univ of Arizona Press, Tucson, AZ), pp 114–143.
2. Bischoff A (1998) Aqueous alteration of carbonaceous chondrites: Evidence for preaccretionary alteration. A review. *Meteorit Planet Sci* 33(5):1113–1122.
3. Lyons JR, Young ED (2005) CO self-shielding as the origin of oxygen isotope anomalies in the early solar nebula. *Nature* 435(7040):317–320.
4. Schulte M, Shock E (2004) Coupled organic synthesis and mineral alteration on meteorite parent bodies. *Meteorit Planet Sci* 39(9):1577–1590.
5. Martins Z, et al. (2008) Extraterrestrial nucleobases in the Murchison meteorite. *Earth Planet Sci Lett* 270(1–2):130–136.
6. Young ED, Ash RD, England P, Rumble D, 3rd (1999) Fluid flow in chondritic parent bodies: Deciphering the compositions of planetesimals. *Science* 286(5443):1331–1335.
7. Palguta J, Schubert G, Travis BJ (2010) Fluid flow and chemical alteration in carbonaceous chondrite parent bodies. *Earth Planet Sci Lett* 296(3–4):235–243.
8. Castillo-Rogez JC, Schmidt BE (2010) Geophysical evolution of the Themis family parent body. *Geophys Res Lett* 37(10):L10202.
9. Casey WH, Banfield JF, Westrich HR, McLaughlin L (1993) What do dissolution experiments tell us about natural weathering? *Chem Geol* 105(1–3):1–15.
10. Endress M, Zinner E, Bischoff A (1996) Early aqueous activity on primitive meteorite parent bodies. *Nature* 379(6567):701–703.
11. de Leuw S, Rubin AE, Schmitt AK, Wasson JT (2009) 53Mn–53Cr systematics of carbonates in CM chondrites: Implications for the timing and duration of aqueous alteration. *Geochim Cosmochim Acta* 73(24):7433–7442.
12. Sears DWG, Hasan EA, Batchelor JD, Lu J (1991) Chemical and physical studies of type 3 chondrites–XI: Metamorphism, pairing, and brecciation of ordinary chondrites. *Proc Lunar Planet Sci Conf* 21:493–512.
13. Bennett ME, McSween HY (1996) Revised model calculations for the thermal histories of ordinary chondrite parent bodies. *Meteorit Planet Sci*, 31(6):783–792, Translated from English.
14. McSween HY, Labotka TC (1993) Oxidation during metamorphism of the ordinary chondrites. *Geochim Cosmochim Acta* 57(5):1105–1114, Translated from English.
15. Hutchison R, Alexander CMO, Barber DJ (1987) The Semarkona meteorite: First recorded occurrence of smectite in an ordinary chondrite, and its implications. *Geochim Cosmochim Acta* 51(7):1875–1882.
16. Grossman JN, Alexander CMOD, Wang J, Brearley AJ (2000) Bleached chondrules: Evidence for widespread aqueous processes on the parent asteroids of ordinary chondrites. *Meteorit Planet Sci* 35(3):467–486.
17. Kovach HA, Jones RH (2010) Feldspar in type 4–6 ordinary chondrites: Metamorphic processing on the H and LL chondrite parent bodies. *Meteorit Planet Sci* 45(2):246–264.
18. Rubin AE, Ziegler K, Young ED (2008) Size scales over which ordinary chondrites and their parent asteroids are homogeneous in oxidation state and oxygen-isotopic composition. *Geochim Cosmochim Acta* 72(3):948–958.
19. Stöffler D, et al. (1986) Shock metamorphism and petrography of the Shergotty achondrite. *Geochim Cosmochim Acta* 50(6):889–903.
20. Clayton RN, Mayeda TK, Goswami JN, Olsen EJ (1991) Oxygen isotope studies of ordinary chondrites. *Geochim Cosmochim Acta* 55(8):2317–2337.
21. Cherniak DJ (2003) Silicon self-diffusion in single-crystal natural quartz and feldspar. *Earth Planet Sci Lett* 214(3–4):655–668.
22. Ryerson FJ, McKeegan KD (1994) Determination of oxygen self-diffusion in åkermanite, anorthite, diopside, and spinel: Implications for oxygen isotopic anomalies and the thermal histories of Ca-Al-rich inclusions. *Geochim Cosmochim Acta* 58(17): 3713–3734.
23. Giletti BJ, Semet MP, Yund RA (1978) Studies in diffusion–III. Oxygen in feldspars: An ion microprobe determination. *Geochim Cosmochim Acta* 42(1):45–57.
24. Farver J, Yund R (1995) Grain boundary diffusion of oxygen, potassium and calcium in natural and hot-pressed feldspar aggregates. *Contrib Mineral Petrol* 118(4):340–355.
25. Kohn MJ (1999) Why most "dry" rocks should cool "wet." (Translated from English). *Am Mineral* 84(4):570–580.
26. Bocharnikov RE, Shmulovich KI, Tkachenko SI, Korzhinskii MA, Steinberg GS (2000) Gas metasomatism: Experiments on natural fumaroles of Kudryavyi Volcano, Iturup, Kuril Islands. *Geochem Int* 38(5):S186–S193.
27. Kessel R, Beckett JR, Stolper EM (2007) The thermal history of equilibrated ordinary chondrites and the relationship between textural maturity and temperature. (Translated from English). *Geochim Cosmochim Acta* 71(7):1855–1881.
28. Hövelmann J, Putnis A, Geisler T, Schmidt B, Golla-Schindler U (2010) The replacement of plagioclase feldspars by albite: Observations from hydrothermal experiments. *Contrib Mineral Petrol* 159(1):43–59.
29. Mora CI, Riciputi LR, Cole DR (1999) Short-lived oxygen diffusion during hot, deep-seated meteoric alteration of anorthosite. *Science* 286(5448):2323–2325.
30. Swindle TD, Grossman JN, Olinger CT, Garrison DH (1991) Iodine-xenon, chemical, and petrographie studies of Semarkona chondrules: Evidence for the timing of aqueous alteration. *Geochim Cosmochim Acta* 55(12):3723–3734.
31. Krot AN, et al. (2006) Timescales and settings for alteration of chondritic meteorites. *Meteorites and the Early Solar System II*, eds Lauretta DS, McSween HY (Univ of Arizona Press, Tucson), pp 525–553.
32. Zolensky ME, et al. (1999) Asteroidal water within fluid inclusion-bearing halite in an H5 chondrite, Monahans (1998). *Science* 285(5432):1377–1379.
33. Fries M, Zolensky ME, Steele A (2011) Mineral inclusions in Monahans and Zag halites: Evidence of the originating body. *74th Annual Meeting of the Meteoritical Society* (Meteoritics and Planetary Science Supplement, London, UK), p 5390.
34. Whitby J, Burgess R, Turner G, Gilmour J, Bridges J (2000) Extinct (129)I in halite from a primitive meteorite: Evidence for evaporite formation in the early solar system. *Science* 288(5472):1819–1821.
35. Busfield A, Gilmour JD, Whitby JA, Turner G (2004) Iodine-xenon analysis of ordinary chondrite halide: Implications for early solar system water. *Geochim Cosmochim Acta* 68(1):195–202.
36. Petitat M, et al. (2011) 53Mn-53Cr ages of Kaidun carbonates. *Meteorit Planet Sci* 46 (2):275–283.
37. Young ED, Coutts DW, Kapitan D (1998) UV laser ablation and irm-GCMS microanalysis of O-18/O-16 and O-17/O-16 with application to a calcium-aluminium-rich inclusion from the Allende meteorite. *Geochim Cosmochim Acta* 62(18):3161–3168.